Draft version March 7, 2022
Typeset using LaTeX default style in AASTeX631

arXiv:2203.01959v1 [astro-ph.GA] 3 Mar 2022

Detection of Gravitational Redshift in Open Cluster non-degenerate stars

Carlos M. Gutiérrez[1] and Nataliya Ramos-Chernenko[1,2]

[1] *Instituto de Astrofísica de Canarias,*
Vía Láctea S/N, E-38205 La Laguna, Tenerife, Spain
[2] *Universidad de La Laguna,*
E-30206 La Laguna, Tenerife, Spain

ABSTRACT

A key observational prediction of Einstein's Equivalence Principle is that light undergoes redshift when it escapes from a gravitational field. Although astrophysics provides a wide variety of physical conditions in which this redshift should be significant, till very recently the observational evidence for this gravitational effect was limited to the light emitted by the Sun and white dwarfs. *Gaia*-DR2 astrometric and kinematic data, in combination with other spectroscopic observations, provides a test bench to validate such predictions in statistical terms. The aim of this paper is to analyze several thousand main-sequence and giant stars in open clusters (OCs) to measure the gravitational redshift effect. Observationally, a spectral shift will depend on the stellar mass-to-radius ratio as expected from the theoretical estimation of relativity. After the analysis, the obtained correlation coefficient between theoretical predictions and observations for 28 (51) OCs is $a = 0.977 \pm 0.218$ (0.899 ± 0.137). The result has proven to be statistically robust and with little dependence on the details of the methodology or sample selection criteria. This study represents one of the more extensive validations of a fundamental prediction of gravity theories.

Keywords: gravitational redshift — stars: main-sequence and late-type — stellar open clusters — gravitation - radial velocities

1. INTRODUCTION

According to the predictions of the Einstein's Equivalence Principle (EEP) the light emitted in the stellar photospheres suffers a redshift when escaping its gravitational field, which is directly correlated to the mass-to-radius ratio of the observed star. In numbers, the measured effect is of the order of several hundred $\mathrm{m\,s^{-1}}$ for main-sequence stars and tens of times smaller for giants. For white dwarfs the gravitational effect is several tens of $\mathrm{km\,s^{-1}}$ owing to their comparatively small radius and extremely massive cores. That explains why the first attempts at detecting this relativistic effect was achieved in these types of stars by Greenstein & Trimble (1967) and Trimble & Greenstein (1972).

The proximity of the Sun allows high-quality observations that are unattainable for other stars. However, since the Sun is a main-sequence star, the gravitational effect is relatively small and the observations need to consider the shift associated with the convective nature of the photosphere. In the solar spectrum, for example, the absorption line wavelength is blueshifted by about 400 $\mathrm{m\,s^{-1}}$ after correction for the known gravitational redshift (Lindegren & Dravins 2003). In general, the precise amount of convective shift depends on the strength of the absorption line, i.e. stellar metallicity, surface gravity, and spectral type, or effective temperature (Allende Prieto et al. 2002, 2013). Several measurements have been made of the Sun (Roca Cortés & Pallé 2014), the most precise estimate being performed by González Hernández et al. (2020), who take into account all these effects to determine the Sun's gravitational redshift at 633.1 $\mathrm{m\,s^{-1}}$ with an uncertainty of $\sim 1\%$.

Extending the test to other non-degenerate stars is of interest in order to test the EEP and the accuracy of stellar models. Nevertheless, as outlined above, such experiments are difficult: on the one hand, the hydrodynamic effect of the stellar photosphere produces a counterbalancing effect that tends to cancel out the relatively small gravitational redshift effect of the typical main-sequence star; on the other hand, obtaining data with high enough quality requires considerable effort in terms of observing time and instrumentation of high spectral resolution. These considerations

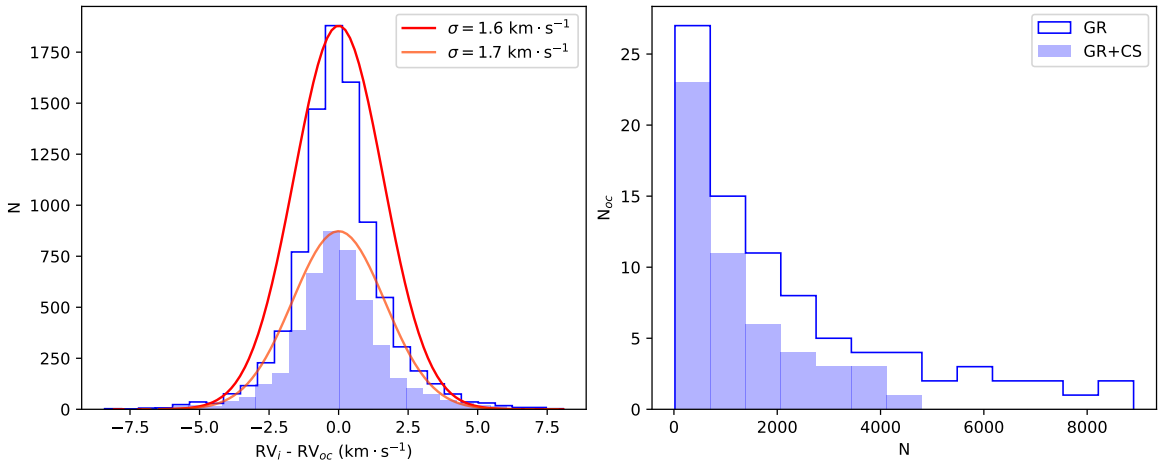


Figure 1. *Left panel*: Distribution of the stellar radial velocities (RV_i) relative to its host cluster ($RV_{\rm OC}$). The solid lines are the Gaussian distribution fits for each sample, with corresponding standard deviations (σ) depicted in the label. N denotes the number of stars. *Right panel*: Histogram distribution of the member stars (N) population in open cluster ($N_{\rm OC}$). In both panels, the step-type histogram corresponds to the full data set of 86 clusters and 8899 stars, labeled GR; the filled histogram corresponds to a subset of 51 clusters and 4464 stars for which it is possible to estimate the convective shift, labeled GR+CS. See main text for details.

explain the relatively low number of such attempts (Nordstroem et al. 1997; Leão et al. 2019; Madsen et al. 2002). Among these, it is worth mentioning the work by Pasquini et al. (2011), who measured the shift of spectral lines for a sample of 144 member stars in the M67 open cluster. The aim was to measure a radial velocity shift difference between the main-sequence and giant stars. The detection was unsuccessful, so the authors conclude that the convective shift probably mimicked the gravitational effect. More recently, Dai et al. (2019) used *Gaia* radial velocity data to measure the redshift in the main-sequence stars and found values that are much smaller than the theoretical predictions. Again, the authors attributed this deficiency to the convective blueshift effect. A more successful attempt to detect the gravitational effect was carried out by Moschella et al. (2021) in non-degenerate stars. These authors measured the differences in velocities between the components of pairs of co-moving stars formed by dwarf–giant binaries. Instead of assuming the stellar hydrodynamical effect, they used a parametric model Allende Prieto et al. (2013) to estimate the convective shift. The final results provide compelling evidence for the compatibility between observations and theoretical predictions. Actually, measuring the gravitational redshift in galaxy clusters (e.g., Cappi 1995; Wojtak et al. 2011; Kaiser 2013) and quasars (Mediavilla & Jiménez-Vicente 2021) could also be used to test General Relativity versus alternative theories of gravitation.

Nowadays, the availability of huge databases with astrometric, photometric and spectroscopic information, such as SDSS and *Gaia* (Gaia Collaboration et. al. 2016), has provided sufficient objects to detect the gravitational redshift in a statistical way. By using a sample of member stars of open clusters catalogued by *Gaia*, we aim to detect the effect of stellar gravitational redshift in non-degenerate stars. The data analyzed contain several thousand non-degenerate stars covering a wide range of mass and radius that potentially allows us to detect relative variations in their gravitational redshift. Unfortunately, the relatively weak gravitational fields existing in non-degenerated stars and the accuracy of the data used in this work does not allow to discriminate between different gravitational theories.

The paper is structured in a standard way. After this introduction, Section 2 describes the sample and methodology used; in Section 3 are presented the analysis, main results, and their interpretation. Finally, conclusions and planned future work are given in Section 4.

2. METHODOLOGY AND SAMPLE

For this study, we use a sample of stars in open clusters (OCs) of our galaxy. OCs are young stellar clusters which have been formed from the same molecular cloud, so their members share roughly the same age and metallicity (Adamo et al. 2020). As co-moving systems bounded by mutual gravitational attraction, their the stellar peculiar velocity in the radial direction may be assumed to be random and to cancel out on average for each OC.

We took advantage of the largest radial velocity (RV) catalogue for stars in OCs by Tarricq et al. (2021). It gathers nearly 30 000 RV measurements of 1382 OC members based on *Gaia*-RVS and ground-based surveys (see references

within). The complete OCs catalogue and the initial membership probability assessment came mostly from Cantat-Gaudin et al. (2020) and Cantat-Gaudin & Anders (2020), both based on *Gaia* DR2 astrometry. The initial 1382 OCs data were completed with stellar parameters from the *Gaia* DR2 based StarHorse catalogue (Anders et al. 2019). This provides estimations of photo-astrometric distances, extinctions, and other astrophysical parameters such as effective temperature ($T_{\rm eff}$), surface gravity ($\log g$) and metallicity ([Fe/H]). The final dataset contains 1342 OCs and 21 403 stars classified as OC members with a minimum membership probability of 0.4, a threshold estimated by the authors. That constitutes the initial data set used in this paper.

In order to select an appropriate subsample for this work, only stars with uncertainties up to 2 $\rm km\,s^{-1}$ in RV measurements were considered. This first restriction removes 24% of the initial sample objects from the analysis, and was motivated by the need to discard not only objects with poor measurements but also those that are part of binary systems, whose velocities could be dominated by the binary orbit itself.

To constrain the stellar membership of the host cluster provided by Soubiran et al. (2018), radial velocities were used as an additional criterion (Nordstroem et al. 1997). It was assumed that the radial velocities of the stars in a given OC correspond to a sample of a Gaussian distribution centred on $RV_{\rm OC}$ with a standard deviation $\sigma_{\rm OC}$. $RV_{\rm OC}$ was estimated as the mean value of the radial velocities of the member stars through an iterative method that rejects as outliers those stars that were originally classified as OC members, but that have velocities outside the $\pm 3\sigma_{\rm OC}$-clipping. It was assumed that the spectral shift corresponds entirely to the motion of the stars, i.e. any other possible contributor, such as the gravitational redshift or convective shift, was ignored at this stage. This approach is likely to produce a small bias (of a few hundred $\rm m\,s^{-1}$) in the estimates of $RV_{\rm OC}$ and $\sigma_{\rm OC}$. The relevance of this minor effect is considered in the results and conclusions sections of this paper.

After estimating the radial velocity for each cluster, two additional restriction were applied. First, we consider only those clusters with a minimum number of stars in order to gain confidence in our estimation of the kinematic parameters of the cluster. Several thresholds were considered and $N_{\rm min} \geq 20$ was chosen as a good option to keep a relatively large sample. To ensure a tight gravitational binding, those clusters with $\sigma_{\rm OC} > 3$ $\rm km\,s^{-1}$ were also discarded. With these restrictions in place, we were left with ∼42% of the original dataset.

Additional properties of the clusters such as morphology, age, position within our galaxy, or the stellar type population, etc., could be also considered as efficient criteria to optimize the sample. However, we decided to ignore them to minimize the number of assumptions and to give a more general validity to the results. Neither has it been considered the information of tangential velocities that should provide a better estimation of the kinematic and dynamical state of the OC. That might constitute an additional criteria to determine the membership probability of the stars[1].

Finally, a total sample of 86 OCs and 8899 stars was selected for further analysis (Table 2). A subsample of 51 OCs and 4464 stars are obtained after applying the restrictions based on the hydrodynamical model to estimate the convective shift effect of the stars (see below). Figure 1 depicts the kinematic and descriptive information for both the GR (step histogram) and GR+CS (filled histogram) data samples. It is expected that the velocity distribution for each cluster follow a Gaussian form, centered on $RV_{\rm OC}$ with a dispersion of $\sigma_{\rm OC}$. In order to consider all the clusters, the relative radial velocity ΔRV distribution was depicted in Figure 1 (*left panel*), subtracting the corresponding $RV_{\rm OC}$. After combining all the clusters, the relative velocity histogram fits a single Gaussian distribution centered at 0 with $\sigma_{\rm GR} = 1.6$ km s^{-1} and $\sigma_{\rm GR+CS} = 1.7$ km s^{-1}, respectively for GR and GR+CS data. The velocity dispersion ranges from -8.41 to 8.08 $\rm km\,s^{-1}$ that roughly corresponds to the ±3-sigma level of the dispersion. The *right panel* shows the histogram distribution of member stars N, illustrating how populated are the clusters ($N_{\rm OC}$). It serves to compare quantitatively the numbers of both data samples.

2.1. *Gravitational Redshift*

To calculate a star's predicted gravitational redshift (GR) it is necessary to know its mass and radius, as $GR \sim M/R$. As a reference value, we estimate the gravitational redshift in the vicinity of the Sun to be $GR_\odot = GM_\odot/cR_\odot = 636.31$[2] $\rm m\,s^{-1}$. Therefore, for a given star of mass M_* and radius R_*, the predicted gravitational effect is given by $GR_* = G(M_*/M_\odot)/c(R_*/R_\odot)$. The stellar masses are provided by StarHorse catalogue (Anders et al. 2019) and their radii can be easily estimated through their surface gravity ($\log g \sim M/R^2$), $\log g$ also being available for each star. The reference value for $\log g_\odot$ is 4.438[2]. Figure 2, *left panel*, illustrates the Hertzprung–Russell (HR) diagram for our total

[1] A further analysis is possible by comparing tangential and radial velocities of the stars, which might provide an alternative way to estimate gravitational redshift.

[2] Calculated using AstroPy astrophysical constants.

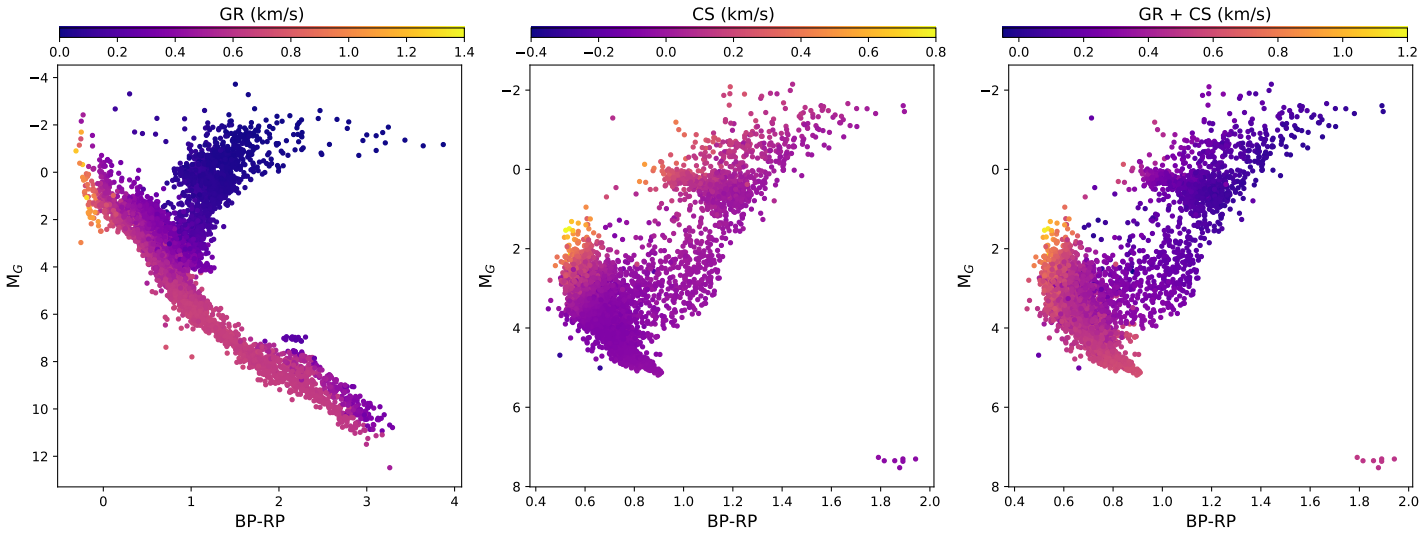


Figure 2. Comprehensive Hertzprung–Russell (HR) diagram with dereddened colors and magnitudes. *Left panel*: 86 clusters and 8899 stars, color-coded by the stars' predicted gravitational redshift (GR) results ($\mathrm{km\,s^{-1}}$). *Middle panel*: 51 clusters and 4464 stars, color-coded by the stars' convective shift (CS) results ($\mathrm{km\,s^{-1}}$). *Right panel*: these 51 clusters and 4464 stars, color-coded by the sum of the GR and CS results ($\mathrm{km\,s^{-1}}$).

data sample, color-coded with the GR predictions ($\mathrm{km\,s^{-1}}$). The GR values span a range from a minimum of 4.45 $\mathrm{m\,s^{-1}}$ for red-giant stars, gradually increasing towards the main-sequence stars with a typical value of 0.60 $\mathrm{km\,s^{-1}}$ and reaching a maximum of 1.30 $\mathrm{km\,s^{-1}}$ for stars above the main-sequence turn-off, some of these being known as blue stragglers (Carrera et al. 2019).

2.2. *Convective Shift*

Convective shift (CS) is a hydrodynamic effect in the observed RV due to the convective motions of the stellar photosphere (Lindegren & Dravins 2003). It produces a net kinematic displacement that is reflected in the line-of-sight velocity shift measured for each star. To estimate the effective contribution of the CS we used the 3D hydrodynamical model developed by Allende Prieto et al. (2013), which is described as a function of three stellar parameters; namely, the stellar effective temperature ($T_{\rm eff}$), surface gravity ($\log g$), and metallicity ([Fe/H]). The model is constrained mainly to the main-sequence (MS) and red-giant-branch (RGB) stellar parameters. The allowed parameter ranges constitute the additional restrictions on the final data set, as mentioned before. The ranges for each parameter are: $T_{\rm eff}[K] \in [3790.0, 6730.0]$; $\log g[dex] \in [9.184 \cdot 10^{-4} * T_{\rm eff} - 2.482, 4.5]$; [Fe/H][dex] $\in [-3.0, 0.0]$.

After the restrictions were imposed, we were left with a total of 51 clusters and 4464 member stars (see Figure 1 for comparison with the initial data set). The estimated CS contribution per star is color-coded in the *middle panel* of the HR diagram (Figure 2). The CS results span a range from a minimum of -322.7 $\mathrm{m\,s^{-1}}$ (i.e. blueshifted) for a typical sun-like star, to a maximum of 804.9 $\mathrm{m\,s^{-1}}$ (i.e. redshifted) for the early F-type dwarfs. It is worth highlighting that less than 2% of the stars have a CS greater than 0.3 $\mathrm{km\,s^{-1}}$, in agreement with the predictions.

The total *velocity shift* contribution to the observed RV, estimated from the sum of the GR and CS effects, is illustrated in the *right panel* of Figure 2. The results are clearly differentiated between the red-giant branch and the main-sequence stars, with a minimum blueshift of -50.84 $\mathrm{m\,s^{-1}}$ and a maximum redshift (for early F-type dwarfs) of 1.16 $\mathrm{km\,s^{-1}}$, respectively. The majority of the sample, namely 74% of stars, have a total predicted shift within the range of 0.2–0.7 $\mathrm{km\,s^{-1}}$.

3. ANALYSIS AND RESULTS

The basic hypothesis taken into account is that the observed spectral shift, in a given star, is a combination of (i) the average radial velocity of its OC; (ii) the radial component of the peculiar velocity of the star within its OC; (iii) the gravitational redshift ($z_{\rm GR}$) which is equivalent from an observational point of view to a radial velocity $GR = cz_{\rm GR}$, and (iv) the effect of the convective shifts (CS) due to the stellar turbulence at the photosphere. The large size and the broad range of stellar parameters in our sample allow us to consider other second-order effects (e.g., the kinematics

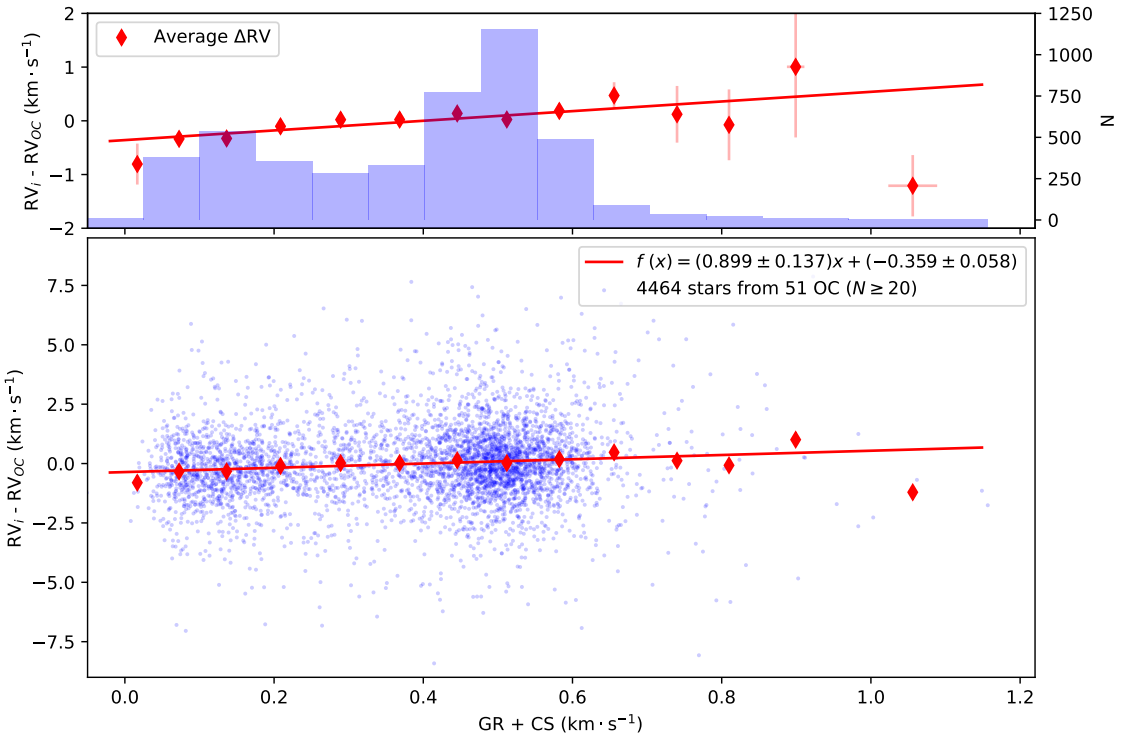


Figure 3. *Upper panel*: Bimodal Histogram of GR + CS (km s^{-1}) for stellar members of 51 OCs ($N \geq 20$), where N is the number of the stars (right Y-axis). The 2-peak distribution shows the presence of the (two) main stellar groups, i.e. red-giants (left) and main-sequence stars (right). *Lower panel*: Linear Regression for $f(x) = \Delta RV$ as a function of x = GR + CS, both in (km s^{-1}). The blue dots represent stellar members of the 51 OCs. In both figures, the red line is the result of a least-squares fit to the 4464 stars; the red diamonds are the binned GR + CS data corresponding to the average value of ΔRV, shown for illustrative purpose only.

of the outer layer, orbital motion in binary systems, etc.) as sources of random noise. The radial velocity of each OC was estimated as the average of the radial velocities of it member stars, while the peculiar velocity of each star within its own OC was also considered a source of random noise. In summary, the observed redshift (after subtracting the mean velocity of the OC) is $\Delta RV = GR + CS + \sigma$. To test this hypothesis, the data was parameterized as $\Delta RV = a \cdot (GR + CS) + b$, where a is the slope correlating the expected results with the observations. Values $a \sim 1$ indicate agreement between theory and observations.

Two different approaches were taken to archive our goal. The first one is based on analyzing a fictitious cluster that has been built through the combination of the stellar members of all the OCs, and analyze it as a single system (hereafter Method A). The second approach considers only the *best*-clusters to analyze them independently (hereafter Method B). In Method A, after subtracting the radial velocity of each cluster, we jointly analyze all the stars of host selected clusters with at least 20 members, i.e. those stars in the step-histograms shown in Figure 1. Method B analyzes OCs with at least 50 members independently. The individual outcome parameters a and b are later combined into a *final* result. The analysis and results for each method are described below.

3.1. *Method A*

First, we ignore the CS contribution and consider our primary data set of 86 OCs and 8899 stars. The aim is to prove, even if without the CS effect, that there is a not-null result when correlating ΔRV with the theoretical GR. Moreover, the CS algorithm was developed specifically for the *Gaia* Radial Velocity Spectrometer (Allende Prieto et al. 2013), while the RV data used have multiple sources (see ref. in Tarricq et al. 2021). To avoid any possible bias from the CS algorithm, it is important first to analyze the GR contribution alone. By least-squares fitting, we perform a linear regression for the ΔRV as a function of GR predictions. The results obtained are: $a = 0.425 \pm 0.077$ (slope) and $b = -0.187 \pm 0.038$ (intercept, or the bias term). This results may be interpreted as a significant correlation between

the observed redshift and the M/R ratio of the stars, although the amplitude of this correlation is about half the value predicted by GRT. As in previous studies, we can associate this difference to the neglected effect of convective shift. The value of b is interpreted as the mean value of the bias associated with the estimation of the radial velocity of each cluster.

In the following, we include in the analysis the CS contribution of each star using the hydrodynamic model proposed by Allende Prieto et al., as explained in the previous section. Figure 3 (*upper panel*) shows the histogram of the GR + CS distribution for these stars. It exhibits a bimodal shape where the peaks correspond to red-giants (left) and main-sequence stars (right). A linear regression was performed for the ΔRV as a function of the sum of GR and CS predictions. Figure 3 (*lower panel*) shows the member stars combined into a single, fictitious cluster and the regression line with a slope $a = 0.899 \pm 0.137$, and intercept $b = -0.359 \pm 0.058$. The value obtained for a is compatible with unity and is therefore consistent with the joint predictions of the GTR and convective shift model. The value of the b parameter may be interpreted as the shift due to the average bias in the estimates of the radial velocities of the clusters (calculated ignoring the GR + CS term of each star). In fact, the mean $\overline{GR + CS}$ for the whole data set (4,464 objects) is 0.383 $\mathrm{km\,s^{-1}}$, compatible with the absolute value of $|b| = 0.359$ $\mathrm{km\,s^{-1}}$.

One of the biggest limitations of this model is the systematic bias that could arise when different types of clusters are combined; for example, combining different clusters having only one-type stellar populations (i.e., either red giants or main-sequence stars). In that case, when subtracting the $RV_{\rm OC}$ (defined as the mean of RV_i, for all i-member stars) and afterwards combining the clusters, any substantial difference between the two stellar types is ruled out. Increasing the number of stars per cluster (N) should avoid this systematic bias. Actually, performing a quick analysis varying the number of stars per combined cluster, we realized that the slope a converges to unity with increasing N. A more conservative analysis would be to perform a linear fit per cluster with a higher N threshold, and then combine the slope results. This analysis has been done in the following section.

3.2. *Method B*

The systematic bias introduced in the estimation of the radial velocity of each OC is a major drawback of Method A. This has motivated the following analysis in which each OC is analyzed individually by estimating the parameters a_j and b_j for each j-OC and then combining their results. In this analysis, the bias in the estimation of the radial velocity of each OC is absorbed in the parameter b_j and does not affect the slopes a_j.

Numerous tests were carried out, changing the threshold for the minimum number of stars, particularly the $N \geq 20$ assumed in Method A. The results obtained are robust against the specific threshold adopted, although the parameters obtained for OCs with relatively low numbers of stars are very noisy and contribute little to the average value. Therefore, a higher limit was applied for this analysis. The following results correspond to a subsample of OCs with at least 50 stars ($N \geq 50$). This restriction reduced the original GR-sample to the *best* 47 OCs with 7713 stars. When the CS contribution is included in the analysis, the complete GR + CS sample is reduced to 28 OCs with 3779 member stars.

The a_j and b_j parameters obtained in the analysis of each OC were weighted according to their respective errors ε_{a_j} and ε_{b_j}. The averaged results, ignoring the CS contribution, are $a = 0.643 \pm 0.164$ and $b = -0.257 \pm 0.067$. The a value obtained is consistent with the non-null hypothesis at $\sim 4\sigma$ level. Modeling the CS effect, the weighted average results are $a = 0.977 \pm 0.218$ and $b = -0.395 \pm 0.082$.

Figure 4 and Table 1 show the a_j results and their standard errors for each OC when considering the CS contribution (the *best*-cluster subsample). The blue- and gray-shaded regions enclose the $a \pm \varepsilon_a$ values obtained from the cumulative mean along the increasing (blue) and decreasing (gray) N values. In both cases it is worth noting the progressive and smooth convergence to the predicted value $a = 1$. Moreover, splitting the data between the most and least populated clusters, should reproduce compatible results within the expected outcome. Combining only the first 18 OCs ($N \leq 150$), we get $a = 1.14 \pm 0.32$, while the last 10 OCs ($N > 150$) give $a = 1.01 \pm 0.32$. Therefore, the analysis of two independent data sets successfully reproduces the predictions.

Although the results for all the OCs show compatibility within the $\pm 3\sigma$ with the $a = 1$ value, the uncertainties in their respective estimations are relatively large and render it impossible to reject the null hypothesis in the analysis of single OCs. Interestingly, the result found in the widely analyzed M67 (NGC 2682) cluster ($a = 1.499 \pm 0.587$, or 1.178 ± 0.388 without modelling the CS contribution) is in tension with previous studies (Pasquini et al. 2011).

In general, the error bars show a strong anticorrelation with the number of stellar members of each OC. However, some of the cases show comparatively higher than expected slopes with low error bars (i.e., Trumpler 5). This could be

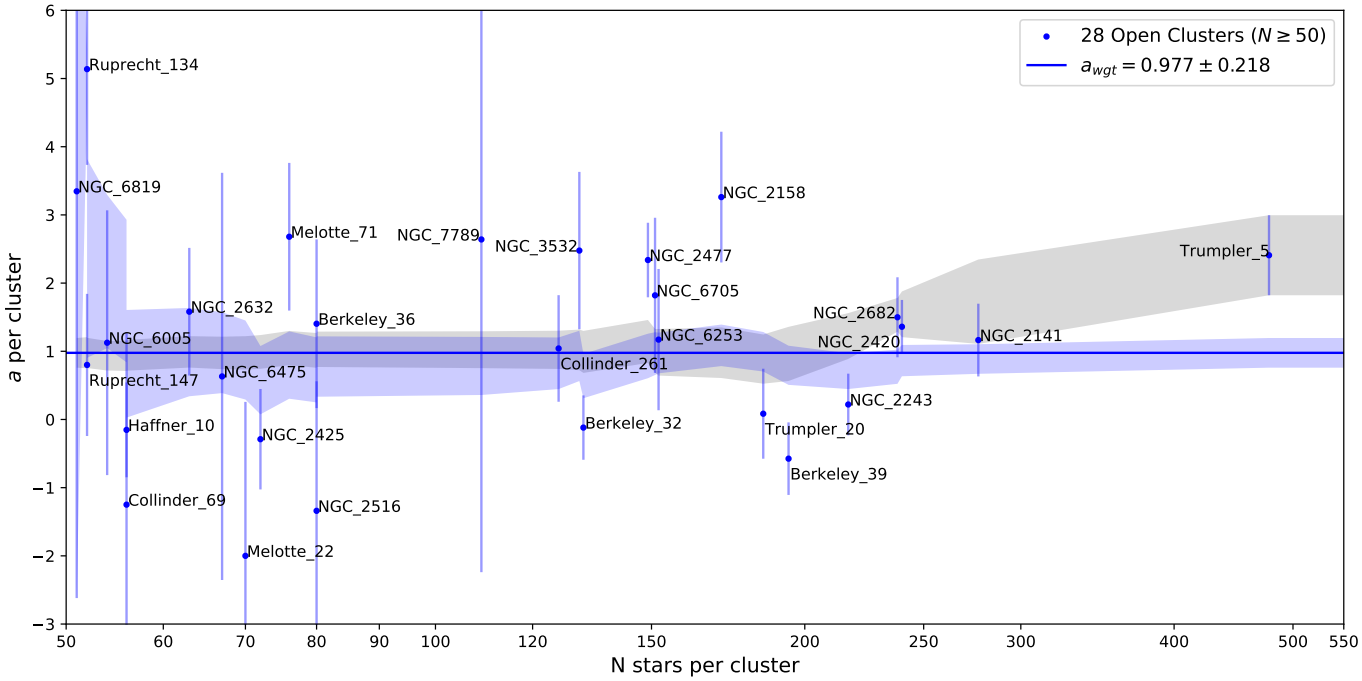


Figure 4. Linear-fit slope (a) as a function of N stars per cluster. The dashed line is the weighted mean slope (a) from the 28 OC ($N \geq 50$) results, with a value of 0.977 ± 0.218. The blue shadow region is the $\pm\sigma$ cumulative weighted average of each OC slope result. Note how the the results converge smoothly to the expected value ($a \sim 1$) with increasing N. The gray shadow region is the the $\pm\sigma$ cumulative weighted average with decreasing N. The error bars are standard deviation errors per cluster. Note that the X-axis is in log-scale for visual clarity.

a consequence of a low ratio of dwarf or giants, kinematic segregation between types, or irregularities in their spatial or kinematic distributions. These hypothesis will require further in-depth study that is beyond the scope of this paper.

4. CONCLUSIONS

The aim of this paper has been to estimate the gravitational redshift in non-degenerate stars, i.e., the light shift when photons escape the gravitational potential of the star, as predicted by the Einstein's Equivalence Principle. This was done by analyzing astrometric, photometric, and spectroscopic information provided mainly by the *Gaia* survey of more than 70 000 non-degenerate stars previously classified as members of galactic open clusters. The study also takes into account information on the spectral shift of the stars (i.e., radial velocities) provided by the ground-based surveys. Radial velocities were assumed to be a combined result of kinematic factors (motion of the OC, peculiar velocity of the stars within its own OC, and convective shift) and the gravitational redshift. When considering each OC, the membership of the stars was re-estimated on the basis of their kinematic information. To ensure the general validity of the results, a minimum number of restrictions on the properties of the OCs and their members was assumed. That gives a baseline sample that contains 86 clusters and 8899 member stars. The main conclusions of the study are the following:

- Ignoring the effect of convective shift, the estimated redshift, which depends on the M/R ratio, is lower in amplitude by roughly a factor of 1.5 than the theoretical expectations from EEP. Similar results were obtained regardless the applied method (A, B).

- By estimating the contribution of convective shift, the original sample is reduced to 51 OCs with more than 20 members each, and a total of 4464 stars. The results show a correlation between predictions and observations as quantified by a significant correlation $a = 0.899 \pm 0.137$. This value is compatible to within 1σ with the predictions (i.e. $a = 1$).

Table 1. Fit results and parameters[i] for OCs with at least 50 members.

Cluster	a	ε_a	b	ε_b	N	RV_{OC}	$\varepsilon_{RV_{OC}}$	σ_{OC}
Trumpler_5	2.409	0.587	−1.014	0.268	478	51.889	0.095	2.293
NGC_2141	1.164	0.533	−0.479	0.229	277	26.802	0.078	1.462
NGC_2420	1.360	0.393	−0.671	0.187	240	74.939	0.049	0.839
NGC_2682	1.499	0.587	−0.640	0.251	238	34.451	0.063	1.093
NGC_2243	0.220	0.452	−0.117	0.200	217	59.929	0.064	1.048
Berkeley_39	−0.575	0.532	0.128	0.215	194	59.053	0.079	1.287
Trumpler_20	0.084	0.660	0.043	0.284	185	−39.553	0.110	1.973
NGC_2158	3.261	0.959	−1.167	0.383	171	28.678	0.186	2.694
NGC_6253	1.171	1.036	−0.395	0.433	152	−28.375	0.102	1.549
NGC_6705	1.820	1.138	−1.083	0.536	151	36.081	0.149	2.597
NGC_2477	2.338	0.547	−0.715	0.192	149	8.155	0.099	1.330
Berkeley_32	−0.119	0.472	0.017	0.192	132	106.216	0.069	0.863
NGC_3532	2.477	1.154	−1.265	0.587	131	5.803	0.067	1.479
Collinder_261	1.041	0.781	−0.243	0.244	126	−24.423	0.094	1.309
NGC_7789	2.640	4.879	−0.192	0.437	109	−54.134	0.124	1.499
Berkeley_36	1.404	1.237	−0.408	0.390	80	63.235	0.163	1.704
NGC_2516	−1.340	1.900	1.002	0.998	80	24.200	0.054	1.067
Melotte_71	2.680	1.083	−1.133	0.482	76	51.811	0.173	1.745
NGC_2425	−0.289	0.737	0.033	0.344	72	104.085	0.113	1.155
Melotte_22	−2.000	2.258	1.283	1.201	70	6.077	0.051	0.998
NGC_6475	0.632	2.986	−0.516	1.483	67	−14.717	0.231	2.180
NGC_2632	1.581	0.936	−1.102	0.482	63	35.459	0.071	0.963
Collinder_69	−1.249	2.518	0.942	0.965	56	28.388	0.170	1.744
Haffner_10	−0.153	0.695	−0.002	0.285	56	87.999	0.114	0.946
NGC_6005	1.126	1.942	−0.203	0.810	54	−24.567	0.279	2.348
Ruprecht_147	0.800	1.042	−0.323	0.534	52	42.397	0.127	1.093
Ruprecht_134	5.138	1.404	−1.141	0.418	52	−39.909	0.221	1.917
NGC_6819	3.346	5.965	−0.309	0.588	51	2.811	0.213	1.592

[i] Values for b, ε_b, RV, ε_{RV} and σ_{OC} are in $\mathrm{km\,s^{-1}}$.

NOTE—The table shows the results obtained for the 28 OCs with at least 50 member stars. OCs are sorted in descending order with N. Table 1 is published in its entirety in the electronic edition of the *Astrophysical Journal*. A portion is shown here for guidance regarding its form and content. The full version includes the results without modelling the CS.

- An improved method applied to the *best*-cluster subsample containing 28 OCs ($N \geq 50$ each) and 3779 stars gives a correlation in accordance with the predictions; namely, $a = 0.977 \pm 0.218$.
- When splitting the complete GR + CS sample of 28 OCs into two independent sets – (i) OCs with lower number of members ($N \leq 150$ per cluster) and (ii) OCs with higher number of members ($N > 150$ per cluster) – the results are $a = 1.14 \pm 0.32$ and $a = 1.01 \pm 0.32$, respectively. This latter approach gives further confidence in the overall results.

In summary, the result is robust since it was extensively tested on a variety of constraints and restrictions used to form the sample. This constitutes one of the widest and more conclusive estimations of gravitational redshift in non-degenerate stars. The result shows the potential of large astronomical observations in testing physical theories and is a step forward toward proving the universal character of physical laws. Potentially, incorporating information on tangential velocities jointly with the radial velocities provided by *Gaia*-DR3, and other ground-based surveys, will

significantly enhance the sample. A better and wider spatial sampling will add further significance to the result of this work.

We thank Y. Tarricq for kindly providing the *RV* data prior to the public release. We also thank M. López-Corredoira and E. Mediavilla for useful comments and insights into several aspects such as methodology and interpretation of this study. We would like also to acknowledge an anonymous referee for his/her useful comments, and in particular those clarifying the scope of the results. This work has made use of data from the European Space Agency (ESA) mission *Gaia* (https://www.cosmos.esa.int/gaia), processed by the *Gaia*Data Processing and Analysis Consortium (DPAC, https://www.cosmos.esa.int/web/gaia/dpac/consortium). Funding for the DPAC has been provided by national institutions, in particular the institutions participating in the *Gaia* Multilateral Agreement. This work was funded by the Agencia Estatal de Investigación (AEI), of the spanish Ministerio de Ciencia e Innovación (MICINN) under the project PID2019-110614GB-C21/AEI/10.13039/501100011033. N.R. also acknowledges support from the AEI and the European Social Fund (ESF) under grant *Ayuda para contratos predoctorales para la formación de doctores* with reference PRE2020-095880.

Facilities: *Gaia* DR2 (Gaia Collaboration et. al. 2016, 2018).

Software: Astropy (Astropy Collaboration et al. 2013, 2018), Pandas (The Pandas Development Team 2020), Matplotlib (Hunter 2007), Statsmodels (Seabold & Perktold 2010), AdjustText (https://github.com/Phlya/adjustText).

APPENDIX

Table 2 provides the information about the radial velocity and the estimation of the GR and CS effect for 8899 stars in 86 clusters.

Table 2. The base sample.

Gaia DR2	RA (J2000)	Dec (J2000)	Cluster	RV[a] (km s^{-1})	σ_{RV}[a] (km s^{-1})	CS (km s^{-1})	GR (km s^{-1})
38354680725946240	58.75658414	12.485542172	Melotte_25	36.265	0.172		0.6780
43538293935879680	58.77775368	16.998372278	Melotte_25	36.509	0.064		0.6675
44894472808190720	55.48191696	18.759813169	Melotte_25	35.201	0.695		0.6357
45142206521351552	61.92550271	15.162689108	Melotte_25	38.500	0.385	0.0769	0.4145
45367056650753280	61.56773091	15.698035581	Melotte_25	37.602	0.184	-0.0881	0.6148

[a]From Tarricq et al. (2021).

NOTE—Table 2 is published in its entirety in the electronic edition of the *Astrophysical Journal*. A portion is shown here for guidance regarding its form and content.

REFERENCES

Adamo, A., Zeidler, P., Kruijssen, J. M. D., et al. 2020, SSRv, 216, 69, doi: 10.1007/s11214-020-00690-x

Allende Prieto, C., Koesterke, L., Ludwig, H. G., Freytag, B., & Caffau, E. 2013, A&A, 550, A103, doi: 10.1051/0004-6361/201220064

Allende Prieto, C., Lambert, D. L., Tull, R. G., & MacQueen, P. J. 2002, ApJL, 566, L93, doi: 10.1086/339658

Anders, F., Khalatyan, A., Chiappini, C., et al. 2019, A&A, 628, A94, doi: 10.1051/0004-6361/201935765

Astropy Collaboration, Robitaille, T. P., Tollerud, E. J., et al. 2013, A&A, 558, A33, doi: 10.1051/0004-6361/201322068

Astropy Collaboration, Price-Whelan, A. M., Sipőcz, B. M., et al. 2018, AJ, 156, 123, doi: 10.3847/1538-3881/aabc4f

Cantat-Gaudin, T., & Anders, F. 2020, A&A, 633, A99, doi: 10.1051/0004-6361/201936691

Cantat-Gaudin, T., Anders, F., Castro-Ginard, A., et al. 2020, A&A, 640, A1, doi: 10.1051/0004-6361/202038192

Cappi, A. 1995, A&A, 301, 6

Carrera, R., Pasquato, M., Vallenari, A., et al. 2019, A&A, 627, A119, doi: 10.1051/0004-6361/201935599

Dai, D.-C., Li, Z., & Stojkovic, D. 2019, ApJ, 871, 119, doi: 10.3847/1538-4357/aaf6aa

Gaia Collaboration et. al. 2016, A&A, 595, A1, doi: 10.1051/0004-6361/201629272

—. 2018, A&A, 616, A1, doi: 10.1051/0004-6361/201833051

González Hernández, J. I., Rebolo, R., Pasquini, L., et al. 2020, A&A, 643, A146, doi: 10.1051/0004-6361/202038937

Greenstein, J. L., & Trimble, V. L. 1967, ApJ, 149, 283, doi: 10.1086/149254

Hunter, J. D. 2007, Computing in Science & Engineering, 9, 90, doi: 10.1109/MCSE.2007.55

Kaiser, N. 2013, MNRAS, 435, 1278, doi: 10.1093/mnras/stt1370

Leão, I. C., Pasquini, L., Ludwig, H. G., & de Medeiros, J. R. 2019, MNRAS, 483, 5026, doi: 10.1093/mnras/sty3215

Lindegren, L., & Dravins, D. 2003, A&A, 401, 1185, doi: 10.1051/0004-6361:20030181

Madsen, S., Dravins, D., & Lindegren, L. 2002, A&A, 381, 446, doi: 10.1051/0004-6361:20011458

Mediavilla, E., & Jiménez-Vicente, J. 2021, The Astrophysical Journal, 914, 112, doi: 10.3847/1538-4357/abfb70

Moschella, M., Slone, O., Dror, J. A., Cantiello, M., & Perets, H. B. 2021, arXiv e-prints, arXiv:2102.01079. https://arxiv.org/abs/2102.01079

Nordstroem, B., Andersen, J., & Andersen, M. I. 1997, A&A, 322, 460

Pasquini, L., Melo, C., Chavero, C., et al. 2011, A&A, 526, A127, doi: 10.1051/0004-6361/201015337

Roca Cortés, T., & Pallé, P. L. 2014, MNRAS, 443, 1837, doi: 10.1093/mnras/stu1238

Seabold, S., & Perktold, J. 2010, in 9th Python in Science Conference

Soubiran, C., Cantat-Gaudin, T., Romero-Gómez, M., et al. 2018, A&A, 619, A155, doi: 10.1051/0004-6361/201834020

Tarricq, Y., Soubiran, C., Casamiquela, L., et al. 2021, A&A, 647, A19, doi: 10.1051/0004-6361/202039388

The Pandas Development Team, e. 2020, pandas-dev/pandas: Pandas (Zenodo), doi: 10.5281/zenodo.3509134

Trimble, V., & Greenstein, J. L. 1972, ApJ, 177, 441, doi: 10.1086/151721

Wojtak, R., Hansen, S. H., & Hjorth, J. 2011, Nature, 477, 567, doi: 10.1038/nature10445